

GaAs/AlOx micropillar fabrication for small mode volume photon sources

John M. Choi, Kevin L. Silverman, Martin J. Stevens,
Todd L. Harvey, and Richard P. Mirin^{a)}

National Institute of Standards and Technology, Boulder, Colorado 80305

(Received 21 May 2009; accepted 7 December 2009; published 20 January 2010)

Micropillar devices have shown promise as single photon sources for applications in quantum key distribution as well as single photon metrology and fundamental science. For higher temperature operation (77 K), a high quality factor (Q) cavity and a small modal volume are necessary for enhanced spontaneous emission. Although high Q 's have been demonstrated, achieving small modal volumes is difficult due to the limited index contrast available from the lattice-matched Bragg layers of GaAs and AlGaAs. However, by wet thermal oxidation of AlGaAs or AlAs layers to amorphous aluminum oxide (AlOx), very high index contrast layers can be obtained. This allows for high reflectivity mirrors with fewer Bragg pairs, resulting in reduced mode volume from reduced penetration of the optical mode within the mirror pairs. The authors apply this method in a GaAs/Al_{0.95}Ga_{0.05}As material system and describe a fabrication process for such devices, utilizing a BCl₃:Cl₂:Ar etch. Photoluminescence measurements of micropillars with three top and five bottom layers are demonstrated. They are measured to have Q 's of 200–400 for approximately 1–3 μm diameters, respectively. These results indicate that high Q devices may be possible while simultaneously reducing the modal volume. © 2010 American Vacuum Society.
[DOI: 10.1116/1.3280163]

I. INTRODUCTION

Light confinement and mode control in optical cavities can be used for the controlled generation of photons as well as to study fundamental photon-atom interactions. These properties are especially useful in the field of single photon sources, and successful demonstration of indistinguishable, single photons has been demonstrated.¹ These single photon sources have applications in quantum key distribution² and single photon metrology as well as in fundamental science. For widespread adoption of such devices in practical applications, reliable operation at higher temperature (for example, 77 K) is desired. InGaAs/GaAs quantum dots (QDs) show promise for higher temperature operation as they maintain their single-emitter behavior to liquid nitrogen temperatures.³ Still, generation of indistinguishable photons requires photon emission before any thermally induced pure dephasing. This will require embedding the QDs in high Q , small mode volume optical cavities to enhance the spontaneous emission rate.⁴ For periodic structures that exploit Bragg reflection, such as photonic crystals or Bragg reflectors, large index contrast is crucial for reducing the volume. While air/semiconductor interfaces can be designed in the lateral direction by etching, index differences in the epitaxial direction are limited by the growth of compatible semiconductors. Fortunately, in the GaAs/AlGaAs material system, the oxidation of AlGaAs with high Al mole fraction (>90%) to form AlOx is a well known phenomenon used to confine current injection in vertical-cavity surface-emitting lasers.⁵ When applied to Bragg reflectors, this process has been shown to result in relatively high Q cavities while reducing

the size,⁶ but few details have currently been published in regard to the fabrication of such devices. Due to the extreme difference in the alloy compositions of the two arsenides, tuning parameters for uniform processing can be difficult. In this article, a complete method is presented with the hope that other researches will be expedited in this area.

II. EXPERIMENT

A. Device fabrication

The pillars were fabricated on a wafer grown by molecular beam epitaxy on a GaAs substrate. The epitaxy structure consisted of five pairs of alternating GaAs (89.3 nm) and Al_{0.95}Ga_{0.05}As (187.5 nm) quarter-wave Bragg layers below, and three pairs above a λ -cavity spacer (357.1 nm) centered at around 1200 nm. Within the λ -cavity, three layers of high density quantum dots with emission peaked at approximately 1200 nm were grown at the center of the cavity. Finally, 500 nm plasma enhanced chemical vapor deposition silicon dioxide was deposited by a commercial vendor.

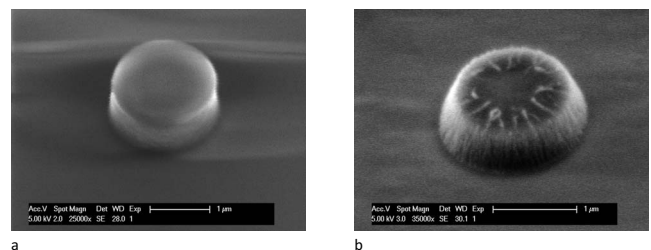


FIG. 1. SEM images of (a) developed photoresist mask and (b) sidewall roughness of the oxide mask after etching.

^{a)}Electronic mail: mirin@boulder.nist.gov

TABLE I. Etch conditions.

Condition	BCl ₃ (SCCM)	Cl ₂ (SCCM)	Ar (SCCM)	ICP (W)	rf bias (W)	P (Pa)	t (min)
1	0	20	10	900	70	0.20	6
2	5	20	10	900	70	0.20	6
3	5	20	10	500	70	0.20	5
4	0	5	15	900	60	0.20	6
5	5	20	10	900	60	0.20	5
6	10	10	10	900	40	0.20	7
7	20	20	20	900	40	0.20	7
8	5	20	10	900	50	0.20	5
9	5	20	10	900	60	0.20	5
10	5	20	10	600	150	0.25	5
11	5	20	10	600	150	0.40	5
12	5	20	10	200	150	0.20	5

Photolithography was performed on a stepper, and then the pattern was transferred into the oxide mask by reactive ion etching (RIE). The oxide etch parameters were 2:1 CHF₃:Ar, 100 W rf for 30 min. Scanning electron microscope (SEM) images are shown in Fig. 1. Although the photomask looks relatively smooth, the oxide etch introduces slight sidewall roughness and slope, which may be transferred into the pillars. Minimal polymer deposition was noticed. The mask was then transferred into the semiconductor using an inductively coupled plasma (ICP) RIE at the UCSB Nanofabrication Facility.

Various etch conditions were tried based on the literature.^{7,8} Some useful results are summarized below and the etch conditions are listed in Table I. Keeping all other parameters constant, the addition of BCl₃ was found to be extremely helpful in obtaining clean etches, as shown in Fig. 2. Although both of the samples are from the same material, the bottom Bragg layers are difficult to see with etch condition 1 [Fig. 2(a)] without BCl₃, while the two Bragg layers above and below the cavity are clear with etch condition 2 [Fig. 2(b)] with BCl₃. The nonuniform etching of the top layers in Fig. 2(b) is most likely due to slope and roughness of the oxide mask [Fig. 1(b)]. To determine if this was due to the AlGaAs, GaAs samples with no epitaxy were also etched,

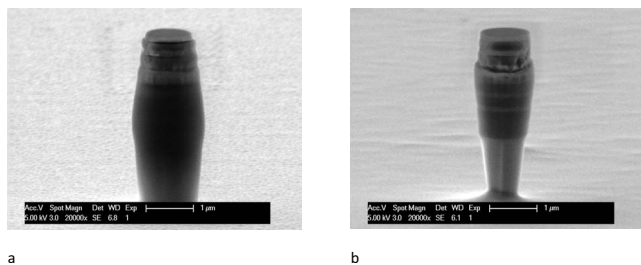


Fig. 2. Addition of a small amount of BCl₃ appears to produce cleaner etches. (a) Etch condition 1, no BCl₃: the bottom Bragg layers are difficult to see. (b) Etch condition 2, with BCl₃: the bottom Bragg layers are clearly visible. The light colored layers are GaAs and the dark colored layers are AlGaAs. The visible layers are (from the top): 2 Bragg pairs (GaAs/AlGaAs), GaAs cavity (light color), 2 Bragg pairs (AlGaAs/GaAs), and a thick AlGaAs layer (3λ/4).

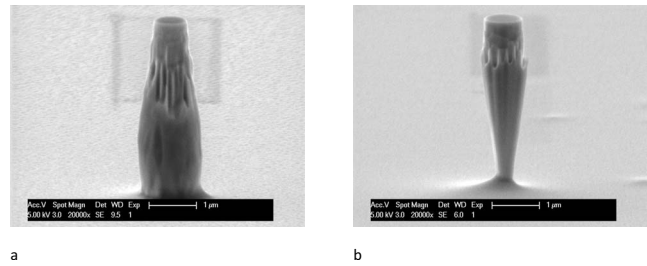


Fig. 3. Effect of BCl₃ etching pure GaAs. (a) Etch condition 1, no BCl₃, and (b) etch condition 2, with BCl₃.

as shown in Fig. 3. Qualitatively, the etches appear similar to Fig. 2, with the bottom half of the pillar appearing rough possibly due to some sort of redeposition, without BCl₃ [etch condition 1, Fig. 3(a)], while the etch looks smooth with BCl₃ [etch condition 2, Fig. 3(b)]. Additional comparisons seemed to indicate that AlGaAs etches slightly slower than GaAs, as seen in Fig. 4. Both samples were etched with the same parameters (condition 3). The GaAs pillar [Fig. 4(a)] appears to be slightly more tapered than the AlGaAs containing pillar [Fig. 4(b)], suggesting that the intermediary AlGaAs layers may be masking the GaAs layers underneath. This effect was only qualitatively observed, and no significant difference in the vertical etch rate was found. For this reason, although most of the etch development can be done with GaAs, it was necessary to check the final etch with the AlGaAs containing material. The cracking of the bottom-most AlGaAs layer is discussed below.

The addition of more Ar resulted in more vertical etches [etch condition 4, Fig. 5(a)] but the etch rate was significantly slow compared to chemistries containing more Cl₂ [etch condition 5, Fig. 5(b)]. Figure 6 shows the effect of increasing the total gas volume while maintaining the chemistry. Figure 6(a) is etched with 10 SCCM (SCCM denotes cubic centimeters per minute at STP) of each gas (condition 6), while the gas flow is doubled for Fig. 6(b) (condition 7) while maintaining the same ratio, resulting in a more chemical etch, as indicated by the increased undercutting of the mask and the pitted sidewalls. Once a suitable chemistry was chosen, adjusting the rf bias controlled the undercut (Fig. 7), resulting in more vertical profiles. Lower rf bias (condition 8) resulted in a more tapered undercut [Fig. 7(a)] than higher bias [condition 9, Fig. 7(b)]. The chamber pressure was im-

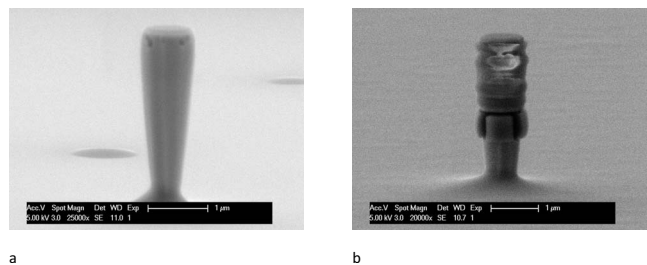


Fig. 4. Compared to (a) GaAs, (b) AlGaAs seems to have a slightly slower etch rate leading to intermediary masking of the GaAs layers (etch condition 3).

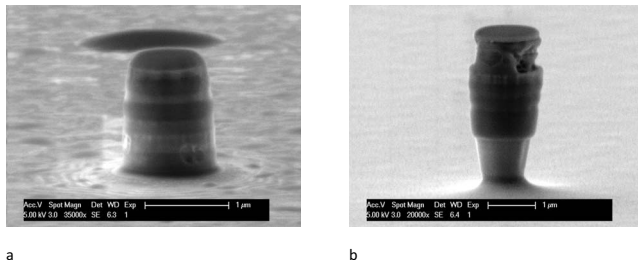


FIG. 5. Increasing the percentage of Ar results in a relatively vertical etch but significantly reduces the etch rate. (a) Etch condition 4, mostly Ar, 6 min etch and (b) etch condition 5, more Cl containing chemistry, 5 min etch.

portant for preventing redeposition of etch products (Fig. 8). Using a pressure of 0.25 Pa (condition 10), the etch appeared free from redeposition [Fig. 8(a)]. However, at a pressure of 0.40 Pa (condition 11), there appears to be some sort of peeling or coating, which is most likely redeposition of etch products [Fig. 8(b)].

Cracking of the AlGaAs layers was found to be a problem. First, thicker layers seemed more susceptible to cracking. In Fig. 4(b), the $\lambda/4$ layers seem unaffected, while the $3\lambda/4$ layer at the bottom has cracked. Empirically, cracking of the quarter-wave layers could be prevented with care, but cracking of thicker layers could not be avoided. Thus, in our final designs, only $\lambda/4$ layers were used. It is believed that the cracking is due to surface oxidation and expansion. This surface oxidation resulted in expansion and split-ring cracking of the thin AlGaAs layers after prolonged exposure for several hours, as seen in Fig. 9(a). Although an exhaustive study was not undertaken, it was found that the short time necessary to remove the etched samples and go into a SEM, about an hour, was insufficient to cause noticeable cracking. An immediate photoresist coat and bake was also attempted to prevent atmosphere exposure. While this slowed down the oxidation rate, noticeable cracking was observed after 2 days, as seen in Fig. 9(b). Ultimately, the best method was to place the etched samples immediately into a high vacuum (10^{-6} Torr) storage container for transport to prevent oxidation and expansion of the Al-containing layers. No noticeable cracking was observed after almost 3 days. The final device etch parameters for $\frac{1}{4}$ of a 3 in. wafer are listed in Table I, condition 12. The etch rate was approximately 640 nm/min with an etch mask selectivity better than 6:1 ($3.2 \mu\text{m}$ etch,

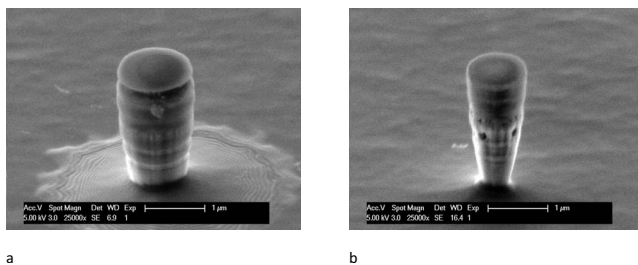


FIG. 6. Increasing the total gas flow with all other parameters constant results in more chemical etching: (a) etch condition 6, 10 SCCM of each gas and (b) etch condition 7, 20 SCCM of each gas.

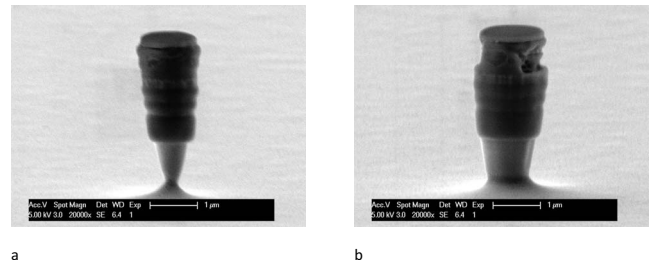


FIG. 7. Increasing rf power of the etch with all other parameters constant results in less undercut and straighter sides: (a) etch condition 8: 50 W (note very tapered tip), (b) etch condition 9: 60 W.

500 nm mask). The etched samples were then wet oxidized in a preheated 450°C furnace.⁹ A round bottom, three neck flask containing de-ionized water was heated up to 70°C by an electric heating mantle with a commercial temperature controller and general purpose resistance temperature detector, and 2 L/min of nitrogen were bubbled through the water using a gas dispersion tube and into the furnace. After 20 min, the nitrogen flow was turned off, and the samples were left in the furnace for an additional 10 min before being removed to cool.¹⁰ The diffusion rate of the oxidation was approximately 200 nm/min. Figure 10 shows the transition between the amorphous AlOx and the crystalline AlGaAs. By measuring the total height of the Bragg layers at the edge of the oxidation boundary, and again beyond the diffusion boundary, we measured shrinkage of 115 nm from an original height of $2.4 \mu\text{m}$. Since the final index contrast is very large, and hence the reflection bandwidth is very large, this small amount of shrinkage was assumed to be negligible since the phase error is approximately 2% per Bragg layer. Finished pillars are shown in Fig. 11. The low quality of the SEM images can be attributed to the insulating oxide layers building up charge.

B. Device measurement

The measurement setup is shown in Fig. 12. The finished samples were placed in a cryostat and cooled to liquid nitrogen temperature (77 K). The pillars were excited with $\sim 100 \mu\text{W}$ from an 808 nm diode laser through a near-IR corrected microscope objective ($\sim 3000 \text{ W/cm}^2$). Due to the extremely large stop band of the oxidized Bragg reflector, it

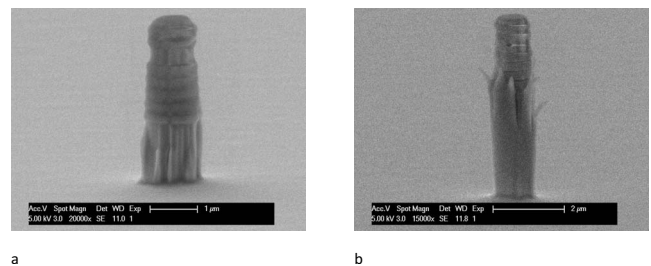


FIG. 8. Increasing the chamber pressure with all other parameters constant (ICP 600 W, $\text{BCl}_3/\text{Cl}_2/\text{Ar}$ 5/20/10 SCCM, rf bias 150 W, 5 min etch) increases the etch rate but seems to result in redeposition: (a) 0.25 Pa and (b) 0.40 Pa (note peeling of possibly redeposited material).

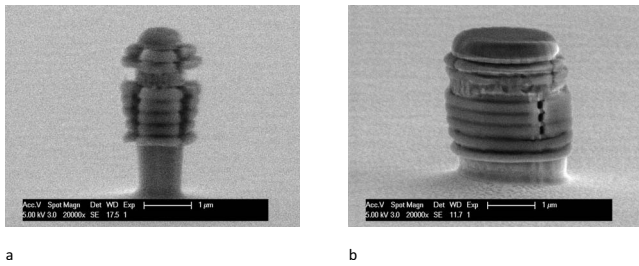


FIG. 9. Cracking of AlAs layers due to oxygen exposure (a) directly in atmosphere and (b) protected by a layer of photoresist immediately after etching.

was difficult to determine the optical power reaching the QD layer. The photoluminescence (PL) was collected through the same objective and filtered through a long-wavelength pass filter to remove the pump before entering a monochromator. The detector signal was then filtered through a lock-in amplifier to obtain the digitized signal. The collected data were fitted to a Lorentzian curve, as shown in Fig. 13. The peak wavelength λ_0 and linewidth $\Delta\lambda$ were then extracted from the Lorentzian lineshape, and the quality factor, $Q = \lambda_0 / \Delta\lambda$, was calculated for each pillar. Several different pillar diameters were examined, having design diameters of 0.75, 1.0, 1.5, 2.0, and 3.0 μm . A minimum of five devices for each pillar diameter were measured.

III. RESULTS AND DISCUSSION

Using a SEM, the devices were imaged along the side to determine the actual width of representative devices. From the images, the measured diameters were 1.2, 1.3, 1.8, 2.3, and 3.3 μm . The peak wavelength of PL is shown in Fig. 14 as a function of the pillar diameter. For each diameter, the peak wavelength is reproducible for different devices, indicating that the fabrication itself is fairly uniform across the measured sample. This is consistent with SEM imaging, which shows little variation in nominally identical pillars on this length scale. The peak wavelength also scales shorter as the pillar diameter becomes smaller, qualitatively matching the expected theoretical behavior of a confined mode. For the largest diameter pillars, many mode peaks could be seen in

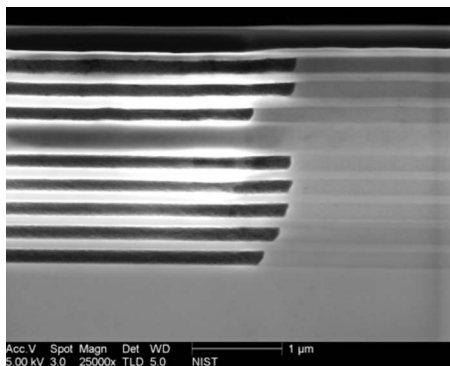


FIG. 10. SEM image showing transition between AlOx (left) and AlAs (right).

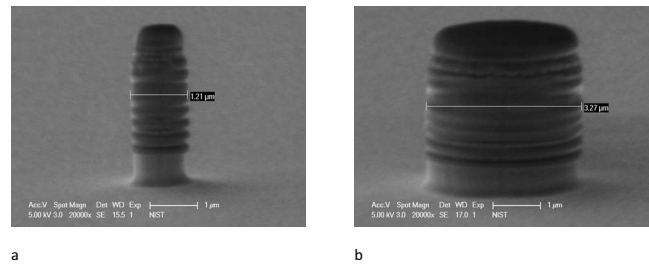


FIG. 11. Final devices (etch condition 12) after wet thermal oxidation of AlGaAs layers (a) 0.75 μm design and (b) 3 μm design.

the PL spectra, indicating that the collection of a particular mode is largely dependent on the spatial location of the collection objective due to variations in the field distribution for higher order modes (Fig. 15).

Figure 16 shows the quality factors of the various pillars measured as a function of the pillar diameters. For pillars with diameters much larger than 3 μm , the PL showed significant multimoded behavior, indicated by multiple, closely spaced peaks of similar intensity. For this reason, it becomes less meaningful to measure the quality factor of the pillar since there are multiple modes with comparable energy content. This may explain the relatively large distribution of quality factors for these largest diameter pillars. Conversely, for the smallest diameter pillars, the photoluminescence intensity was considerably lower due to the smaller emitter size, resulting in a lower signal-to-noise ratio. This indicates that the numerical aperture of our system was not sufficient to capture all of the emission. Thus, the slight increase in the quality factor for the smallest pillars cannot be reliably compared to the next larger sized pillars without further investigation, but should only be considered as showing the general trend of decreasing quality factor with smaller diameter in this experiment, and included for completeness. The Q of the devices measured is substantially smaller than the planar cavity due to scattering at the rough sidewalls, but may also be degraded due to unsaturated quantum dots acting as loss centers. However, the high density of quantum dots ensures a more reproducible result by increasing the signal-to-noise ratio.

Figure 17 shows a simulation of the empty cavity reflectivity of an ideal planar cavity. The stop band width ($>50\%$ reflectivity) is ~ 680 nm. The empty cavity Q is ~ 1600 . The maximum Q that we measure is ~ 400 , a factor of 4 lower than simulated. This reduced Q in the fabricated device is to be expected. The simulated, ideal planar structure includes

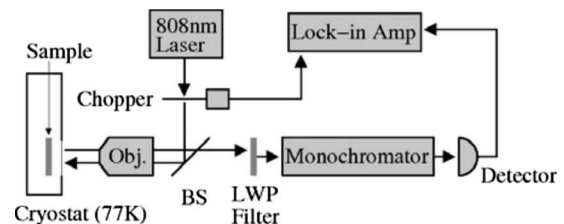


FIG. 12. Experimental setup.

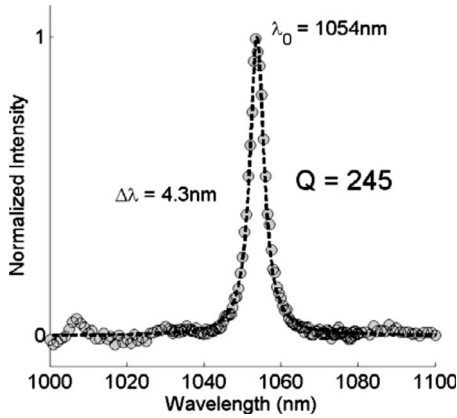


FIG. 13. Photoluminescence data with Lorentzian fit of 2 μm design diameter pillar.

no additional losses due to sidewall scattering in an etched pillar nor losses due to unpumped QDs. However, the fabricated specimens do have these additional losses to reduce their Q 's. For comparison, the structures in Ref. 6 are reported to have an ideal planar Q of $\sim 15\,000$ and a maximum measured Q between 2000 and 3000, a factor of 5–6 lower.

IV. CONCLUSION

A baseline fabrication process for high index contrast micropillars has been developed and presented. The AlGaAs layers create some difficulties due to the reactive nature of the aluminum before wet thermal oxidation, as seen in the cracking and split rings. By using the wet thermal oxidation process to take advantage of the aluminum oxide, a large index contrast can be created in the epitaxial direction. This reduces the modal volume in the vertical direction and fewer Bragg mirror pairs are required. Our design of three top pairs and five bottom pairs results in Q -factors between 200 and 400, while previous work⁶ has shown that four top and seven bottom pairs result in Q -factors between 1000 and 2000 experimentally, and a theoretical planar cavity Q of around 15 000. While higher Q -factors (exceeding 150 000) have

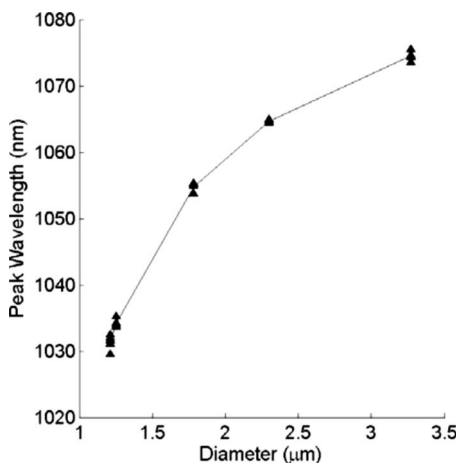


FIG. 14. Peak wavelength (lowest mode) vs pillar diameter with a line through the average of each diameter grouping.

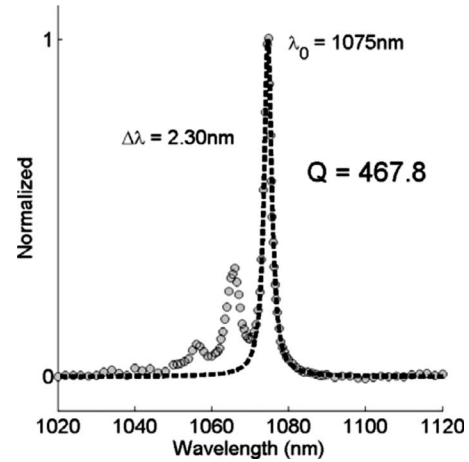


FIG. 15. Photoluminescence data of a $>3\ \mu\text{m}$ diameter pillar with Lorentzian fit of lowest mode exhibiting higher order mode peaks.

been demonstrated, those devices require many more Bragg mirror pairs (approximately 30 pairs on each side of the cavity).¹¹ Previous calculation⁶ shows approximately half an order of magnitude increase in reflectivity for each GaAs/AIOx mirror pair added and predict that six to eight GaAs/AIOx pairs are needed to match the reflectivity of 30 GaAs/AlGaAs mirror pairs. This is consistent with our Q results being about five times less (half an order of magnitude) since we use one to two fewer mirror pairs on each side of the cavity. Thus, we hope that others will be able to use the methods described herein to continue the development of GaAs/AIOx micropillars, with the goal of reaching comparable Q 's with GaAs/AlGaAs micropillars with fewer Bragg mirror pairs and thus smaller mode volumes. Photoluminescence measurements show that the devices are very reproducible based on the peak wavelength of the lowest order mode, most likely due to our choice to use a high density of quantum dots as opposed to the low density of previous work.⁶ However, sidewall roughness, possibly transferred from the oxide mask [Fig. 1(b)], and the high density of

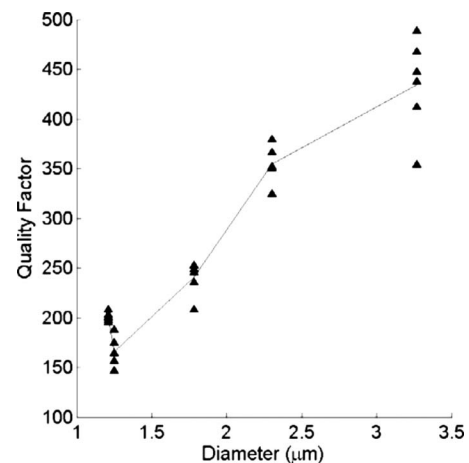


FIG. 16. Quality factor from Lorentzian fit vs pillar diameter with a line through the average of each diameter grouping.

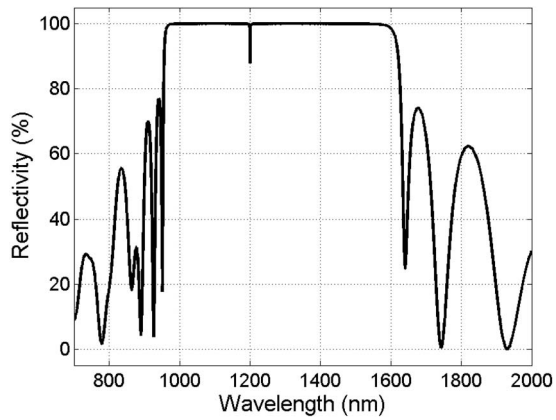


FIG. 17. Simulation of the empty cavity structure including the Bragg mirrors and cavity spacer show that the stop band of the cavity is extremely wide (~ 680 nm) with an ideal Q of 1620.

quantum dots acting as absorbers, due to nonuniform excitation, are the most likely candidates in limiting the Q -factors, resulting in a large variability of Q between devices of the same diameter. However, we have demonstrated the potential of high reflectivity mirrors using only a few number of mirror pairs. This would considerably reduce the mode volume in the epitaxial direction. Once this goal has been achieved, lateral confinement would be facilitated due to the decreased

material thickness that would need to be structured, owing to the fewer Bragg pairs necessary for a given reflectivity.

ACKNOWLEDGMENTS

One of the authors (J.C.) thanks B. Thibeault, D. Freeborn, and the staff at the UCSB Nanofabrication Facility for helpful discussions and facilities access. A portion of this work was done at the UCSB Nanofabrication Facility, part of the NSF funded NNIN network. This work was supported by a grant from the Intelligence Community's Postdoctoral Research Fellowship Program.

¹C. Santori, D. Fattal, J. Vuckovic, G. S. Solomon, and Y. Yamamoto, *Nature (London)* **419**, 594 (2002).

²P. M. Intallura, M. B. Ward, O. Z. Karimov, Z. L. Yuan, P. See, A. J. Shields, P. Atkinson, and D. A. Ritchie, *Appl. Phys. Lett.* **91**, 161103 (2007).

³R. P. Mirin, *Appl. Phys. Lett.* **84**, 1260 (2004).

⁴J. M. Gerard, B. Sermage, B. Gayral, B. Legrand, E. Costard, and V. Thierry-Mieg, *Phys. Rev. Lett.* **81**, 1110 (1998).

⁵D. L. Huffaker, D. G. Deppe, K. Kumar, and T. J. Rogers, *Appl. Phys. Lett.* **65**, 97 (1994).

⁶A. J. Bennet, D. J. P. Ellis, A. J. Shields, P. Atkinson, I. Farrer, and D. A. Ritchie, *Appl. Phys. Lett.* **90**, 191911 (2007).

⁷G. Franz, C. Hoyler, and J. Kaindl, *J. Vac. Sci. Technol. B* **14**, 126 (1996).

⁸G. Franz, *J. Vac. Sci. Technol. A* **16**, 1542 (1998).

⁹K. D. Choquette *et al.*, *IEEE J. Sel. Top. Quantum Electron.* **3**, 916 (1997).

¹⁰R. Y. Li, Z. G. Wang, B. Xu, P. Jin, X. Guo, and M. Chen, *Appl. Phys. A: Mater. Sci. Process.* **86**, 19 (2007).

¹¹S. Reitzenstein *et al.*, *Appl. Phys. Lett.* **90**, 251109 (2007).